Dalton Transactions

ROYAL SOCIETY OF CHEMISTRY

PAPER

View Article Online
View Journal | View Issue

Check for updates

Cite this: *Dalton Trans.*, 2023, **52**, 13190

Blue-LED activated photocatalytic hydrogenation of nitroarenes with Cu_2O/CuO heterojunctions†

Ignacio Chamorro-Mena, Noemi Linares * and Javier García-Martínez *

Received 31st May 2023,
Accepted 31st July 2023

DOI: 10.1039/d3dt01670f

rsc.li/dalton

This study describes how the optimization of Cu_2O/CuO heterostructures can enhance their (photo)catalytic performance. More specifically, the evaluation of catalysts with different Cu_2O/CuO molar ratios was used to optimize their performance for the hydrogenation of 4-nitrophenol under both blue-LED light and dark conditions. For the first time, we analyzed the effect of blue LED irradiation on this reaction and found that when blue LEDs are used as the light source, a Cu_2O/CuO ratio of 0.15 results in rate constants 7 to 3 times higher than those of catalysts with either lower (0.01) or higher (0.42) ratios. Furthermore, this photocatalyst shows good stability, >70% after 5 cycles, and excellent chemoselectivity in the selective reduction of the nitro group in the presence of other functionalities, *i.e.* –COOH, $–CONH_2$ and –OH.

Introduction

The hydrogenation of nitroarenes to anilines is a particularly useful reaction due to the essential role that anilines play as intermediates in the synthesis of pharmaceuticals and dyes.[1] Furthermore, nitroarenes, including nitrophenols, are hazardous pollutants that are extensively generated as waste in agricultural and industrial activities.[2] Therefore, their conversion into the aforementioned aniline intermediates is highly desirable. The most common strategy for achieving this goal involves the catalytic hydrogenation of nitroarenes, which typically requires the use of precious metals as catalysts under high-pressure hydrogen conditions.[1,3,4] In addition to the use of scarce highly costly metals, the chemoselectivity of this reaction is quite poor, as noble metals not only catalyze the hydrogenation of the nitro group but also of other functional groups such as –OH, –C═C, –Cl or –C═O.[5] In this regard, Corma *et al.* reported that by supporting the noble metals (Pt, Ni or Ru) on TiO_2, the chemoselectivity of this reaction is significantly improved because the metal/support interaction favours the adsorption of the nitro group on the metal over the other functionalities.[6] On the other hand, hydrogenation of nitroarenes can be achieved through the use of hydrogen donors such as $NaBH_4$. One advantage of using $NaBH_4$ is that it allows for hydrogenation to occur in aqueous media and eliminates the need for high-pressure equipment.[7] Additionally, this method can utilize more abundant and cost-effective metals or metal oxides as catalysts,[8,9] with copper and copper oxide being among the most effective catalysts.[10,11]

Efforts to develop catalytic processes that are more sustainable and cost-effective are essential from both economic and environmental standpoints. In this sense, utilizing photocatalytic synthetic routes, which rely on light as an energy source to drive chemical reactions, can offer a more sustainable alternative. Since the 1970s, photocatalysis has been extensively researched and applied in various fields, including water splitting, air and water purification, N_2 fixation, and CO_2 reduction, among others.[12] Titanium dioxide (titania) is one of the most versatile and effective semiconductor photocatalysts used in a variety of reactions. It has shown almost quantitative yields of the corresponding anilines for basic nitroarenes, making it an excellent option for this reaction.[13,14] However, using titania as a photocatalyst has a significant drawback – its low activity in the visible spectral range. Therefore, one needs to use ultraviolet light sources or dope the titania surface with metals and/or organics, which can substantially increase the procedure's cost and complexity. Recently, the use of other semiconductors that are less photocatalytically active than titania but respond in the visible range has been explored.[15–17] Examples of such semiconductors are CuO and Cu_2O, which have been tested as photocatalysts in various reactions.[15,16,18] However, despite their advantages such as low cost, versatility, non-toxicity and good response under visible light, they have not yet been evaluated for the photoinduced hydrogenation of nitroarenes to the best of our knowledge.

Here, we explore the use of Cu_2O/CuO heterojunctions, obtained *via* the controlled calcination of the Cu(BTC) MOF (or HKUST-1), for the photocatalyzed hydrogenation of nitro-

Laboratorio de Nanotecnología Molecular, Departamento de Química Inorgánica, Universidad de Alicante, Ctra. San Vicente-Alicante s/n, E-03690 San Vicente del Raspeig, Spain. E-mail: noemi.linares@ua.es, j.garcia@ua.es; https://www.nanomol.es

†Electronic supplementary information (ESI) available. See DOI: https://doi.org/10.1039/d3dt01670f

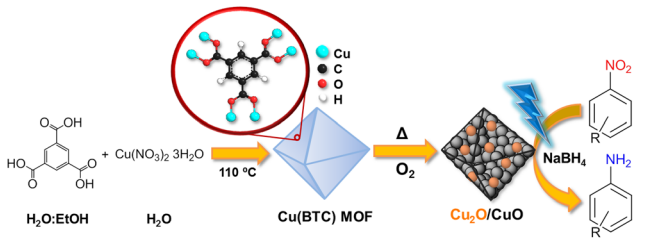

Fig. 1 Schematic representation of the photocatalytic reduction of nitroarenes into aminoarene derivatives by using Cu_2O/CuO catalysts derived from the calcination of the Cu(BTC) MOF.

arenes. More specifically, we evaluated a series of Cu_2O/CuO materials with different molar ratios at 25 °C under both dark and blue-LED light (6 W) conditions using $NaBH_4$ as a hydrogen donor to assess the role of visible light in the enhancement of the rate constant of the reaction (see Fig. 1 for a schematic representation). Under both dark and irradiation conditions, we observed a maximum in the performance of heterojunctions with intermediate Cu_2O/CuO ratios. The use of light is able to enhance the catalytic activity even further, provoking a 2-fold increase in the rate constant compared to the experiments under dark conditions.

Experimental

Materials

All reagents were commercially available and used without further purification. For the synthesis of the Cu(BTC) MOF, we used copper nitrate trihydrate ($Cu(NO_3)_2{\cdot}3H_2O$, 99%) provided by Acros Organics and trimesic acid (benzene-1,3,5-tricarboxylic acid, $C_9H_6O_6$, 95%) supplied by Sigma-Aldrich. Part of the nitrophenols employed in the catalytic tests, more specifically, 2-nitrophenol ($C_6H_5NO_3$, 99%) and 4-nitrophenol ($C_6H_5NO_3$, 99%), were purchased from Thermo Scientific, while the rest of the reagents used for the catalytic evaluation such as sodium borohydride ($NaBH_4$, 96%), 4-nitrobenzoic acid ($C_7H_5NO_4$, 98%) and 4-nitrobenzamide ($C_7H_6N_2O_3$, 98%) were purchased from Sigma-Aldrich.

Preparation of the Cu(BTC) precursor

The Cu(BTC) MOF, also known as HKUST-1, was prepared following a hydrothermal procedure reported elsewhere.[19] Briefly, copper nitrate trihydrate ($Cu(NO_3)_2{\cdot}3H_2O$, 3.1 g) was dissolved in 125 mL of deionized water in a beaker. Separately, benzene-1,3,5-tricarboxylic acid (trimesic acid, 2.0 g) was dissolved in a mixture of deionized water and absolute ethanol in a 1 : 1 v : v ratio. Both solutions were combined and stirred until a homogeneous solution was obtained, which was then transferred to an autoclave and kept in an oven at 110 °C for 18 hours. After that, the autoclave was cooled down naturally to room temperature. Fine blue crystals were obtained, which were isolated by centrifugation and washed with deionized water and subsequently with absolute ethanol.

Cu_2O/CuO catalyst preparation

The Cu_2O/CuO catalysts were obtained by calcination of Cu (BTC) in air. More specifically, 0.5 g of this MOF was calcined for 2 hours at 300 and 400 °C and an additional sample was calcined for 1 hour at 350 °C and then for another 1 hour at 450 °C at a heating rate of 2 °C min^{-1}, to obtain the various materials used as catalysts in this study. Solids were named "Cu_2O/CuO = X," where "X" is the molar ratio that each prepared catalyst presents, with "**Cu_2O/CuO = 0.42**" being the solid obtained from calcining the MOF at 300 °C, "**Cu_2O/CuO = 0.15**" being the solid obtained from calcining at 400 °C and "**Cu_2O/CuO = 0.01**" being the material obtained by calcining with a double ramp.

Sample characterization

The morphology of the materials was investigated by field emission scanning electron microscopy (FESEM) using a Merlin VP compact microscope from Zeiss, at 10 kV, placing the samples on a SEM stub mount with carbon double-tape. Before analysis, the samples were coated with a thin layer of carbon. The size of the primary nanoparticles was studied by transmission electron microscopy (TEM) while the crystalline structure of the heterojunctions was analyzed by selected area electron diffraction (SAED). TEM-SAED analysis was carried out using JEOL JEM-1400 Plus instrument. Samples were suspended in ethanol and sonicated for 10 minutes. A few drops of this suspension were placed on a Lacey Formvar/carbon copper grid. Ethanol was allowed to evaporate at room temperature. The digital analysis of the TEM and SAED micrographs was done using Gatan Digital Micrograph 3.6.1.

The crystallinity of the materials was characterized by X-ray powder diffraction (XRD) in a SEIFERT 2002 apparatus from 20 to 80° 2θ using a scanning velocity of 1° min^{-1} and CuK_α (1.5418 Å) radiation. We analyzed the diffractograms using the X'Pert HighScore Plus software package, which enabled us to identify and quantify the various phases obtained by comparing them with the standard Powder Diffraction Files of the International Center for Diffraction Data (ICCD).

The evolution of the Cu_2O/CuO ratio on the catalysts' surface was studied by X-ray photoelectron spectroscopy (XPS). These measurements were carried out using VG-Microtech Multilab instrument, with MgK-alpha radiation at an energy of 1253.6 eV and a pass energy of 50 eV. The analysis pressure during data acquisition was 5×10^{-7} Pa. The deconvolution of the spectra was made and the obtained areas under the peaks were estimated by calculating the integral of each peak after subtracting a Shirley background and fitting the experimental peak to a combination of Lorentzian/Gaussian lines with a proportion of 30% to 70%. Binding energies were referenced to the C 1s line at 284.6 eV from adventitious carbon.[20]

Diffuse reflectance ultraviolet-visible (DRUV) spectroscopy was used to study the optical properties of the copper oxides obtained from the MOF calcination. DRUV spectra were

obtained in air, at room temperature, and in the range 1200–200 nm using a Shimadzu UV-2401 PC spectrophotometer. $BaSO_4$ was used as the reference material.

The UV-Raman spectra were obtained to further monitor the changes in the crystalline structure. The analyses were carried out on a Jasco NRS-5100 dispersive Raman spectrometer using a 632 nm He–Ne laser source.

The porosity of the catalysts was evaluated by N_2 physisorption at 77 K. The adsorption/desorption isotherms were obtained in a Quadrasorb-Kr/MP apparatus from Quantachrome Instruments. The samples were previously degassed for 12 h at 120 °C at 5×10^{-5} bar. Adsorption data were analyzed using QuadraWinTM (version 6.0) software from Quantachrome Instruments. BET surface areas were calculated using the BET equation.

Catalytic evaluation

The catalytic performances of the various Cu_2O/CuO heterojunctions obtained by the thermal oxidation of Cu(BTC) were evaluated for the reduction of 4-nitrophenol with $NaBH_4$. More specifically, 10 mg of catalyst was added to 135 mL of a 7.4×10^{-2} mM nitroarene aqueous solution, and 20 mL of a 0.06 M solution of $NaBH_4$ in water was used as the reducing agent. First, the nitroarene solution was stirred at 25 °C at 100 rpm using a magnetic stirrer. Subsequently, the catalyst was added, and after homogeneous dispersion, a freshly prepared sodium borohydride solution was added to the mixture. For experiments involving light, the lamp was switched on at the instant of adding borohydride, and the reaction time was recorded from that point forward. At various intervals, 2 mL aliquots were withdrawn and filtered using syringe filters. The conversion of nitrophenol was evaluated by monitoring the gradual decrease in the maximum absorption peak of the nitrophenolate ion at 400 nm. Absorbance measurements were taken in the 200–600 nm range using a Jasco Analytica V650 UV-vis spectrometer. In the experiments conducted under blue-LED irradiation, a blue-LED ring lamp (435–445 nm, Sigma-Aldrich) was used. Experiments were conducted three times to ensure the reproducibility of the results, whereas to evaluate recyclability, the solids were separated by centrifugation after each catalytic cycle and washed with water. A new nitroarene solution was then added to start a new catalytic cycle.

The chemoselectivity of the best perfoming catalytic system was evaluated by reducing nitroarenes containing diverse functional groups. An identical procedure was used to monitor the hydrogenation of the various nitroarenes, and a mass spectrometer was used for the analysis. Specifically, an Agilent Model 1100 Series high-performance liquid chromatograph coupled simultaneously with a variable wavelength visible-UV detector and an Agilent Model 1100 Series LC/MSD Trap SL mass spectrometer with an ion trap analyzer and MS/MS capability were used, with a mass range of 50 to 3000 uma.

Photocatalytic *vs.* catalytic hydrolysis of sodium borohydride

The evaluation of the hydrolysis of sodium borohydride was carried out under both dark and irradiation conditions. The tests were conducted using the best performing catalyst as follows: the catalyst (10 mg) and a magnetic stir bar were introduced into a sealed 100 mL Schlenk flask. This flask was connected to an inverted volumetric tube filled with water. Separately, sodium borohydride (50 mg; 1.32 mmol) was dissolved in 20 mL of water. To start the test, the freshly prepared sodium borohydride solution was injected into the flask and the magnetic stirring was activated (1500 rpm). The flask was tightly wrapped in aluminum foil to prevent the entry of external light. The hydrogen generated was measured by recording the displacement of the liquid in the volumetric test tube.[21] Experiments were conducted at 25 °C using blue LEDs or without light, as required. Each experiment was repeated at least three times to ensure reproducibility.

Results and discussion

The synthesis of Cu(BTC) was monitored by XRD (Fig. 2) and FESEM analysis (Fig. 3). Both techniques confirmed the formation of a high-quality MOF, which was later calcined at different temperatures in air to prepare the Cu_2O/CuO catalysts. The temperature of this treatment was used to control the proportions of Cu_2O and CuO formed. More specifically, the Cu_2O/CuO ratio decreases at higher temperatures, as evidenced by XRD (Fig. 2A), XPS (Fig. 2B) and Raman spectra (Fig. 2C). To track the evolution of the Cu_2O/CuO ratio in the catalysis, we employed the standard XRD cards of the reference metal oxides, tenorite (CuO – JCPDs #48-1548) and cuprite (Cu_2O – JCPDs #77-0199), obtained from the International Center of Diffraction Data (ICDD), and the X'Pert HighScore software package.[22] Our observations revealed that the Cu_2O/

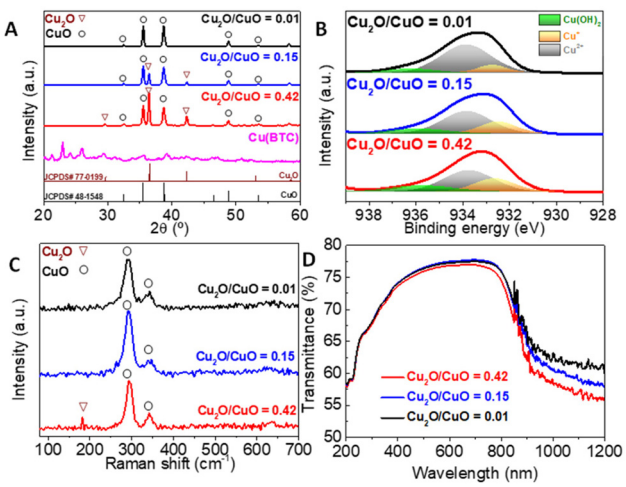

Fig. 2 Physico-chemical characterization of the obtained MOF-derived Cu_2O/CuO materials: (A) XRD patterns of copper oxide catalysts and the Cu(BTC) reference material, (B) deconvoluted Cu $2p_{3/2}$ XPS spectra, (C) UV-Raman spectra and (D) DRUV spectra of the samples: (pink) Cu(BTC), (red) Cu_2O/CuO = 0.42, (blue) Cu_2O/CuO = 0.15 and (black) Cu_2O/CuO = 0.01.

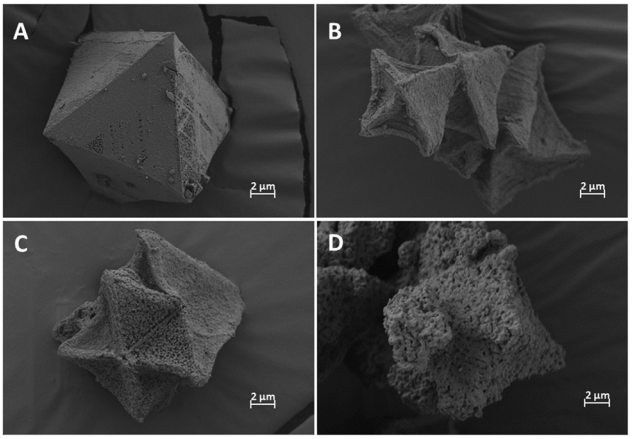

Fig. 3 FESEM micrographs of (A) Cu(BTC), (B) Cu_2O/CuO = 0.42, (C) Cu_2O/CuO = 0.15 and (D) Cu_2O/CuO = 0.01.

CuO ratio shifted from 0.42 at 300 °C to 0.15 at 400 °C. Upon calcination for 1 h at 350 °C and then for another 1 h at 450 °C, the Cu_2O peaks became almost non-existent, resulting in a ratio of 0.01. Raman spectra (Fig. 2C) also confirm the presence of cupric oxide in all calcined samples (peaks at 290 and 340 cm^{-1}) and a small portion of cuprous oxide (200 cm^{-1}) in the sample with a Cu_2O/CuO ratio of 0.42 (in red).[23] SAED analyses were carried out to further analyze the crystalline evolution of the heterojunctions, Fig. S1.† For all materials, the SAED patterns obtained from TEM images at low magnifications exhibit a set of bright rings, which are characteristic of polycrystalline materials. From the reciprocal of the radius of the SAED rings, the interplanar distances can be determined and, by comparison with the standard XRD cards of Cu_2O and CuO, we could identify specific diffractions of the different planes of both oxides (gold rings correspond to Cu_2O while white rings correspond to CuO), see Fig. S1.†

The XPS spectra shown in Fig. 2B confirm a similar Cu_2O/CuO evolution on the surface of the catalysts. The Cu $2p_{3/2}$ spectra reveal a decrease in both the area and size of the peak corresponding to Cu(I) in the lattice (932 eV) as the temperature increases. Meanwhile, the peak corresponding to lattice Cu(II) (933 eV) becomes larger. In all cases, there is also a small peak at 936 eV due to Cu bound to –OH groups, which is usually attributed to water adsorbed on the surface of this material.[24] The diffuse reflectance UV-vis (DRUV) spectra of the solids indicate similar optical absorption properties in all the Cu_2O/CuO photocatalysts produced by thermal oxidation of Cu(BTC) (Fig. 2D). In all cases, a broad absorbance region spanning in the 250–1200 nm range was observed, with an absorption edge at approximately 850 nm for all the Cu_2O/CuO heterostructures. These results suggest that the materials possess excellent light harvesting properties in the visible light range.

As shown in Fig. 3, the FESEM micrographs clearly demonstrate that there are significant changes in the morphology and texture of the samples as the calcination temperature increases. Initially, the materials consisted of perfectly octahedral Cu(BTC) particles with a smooth surface (Fig. 3A). After calcination, the particles retained their octahedral morphology, but their texture became much rougher and more porous due to the formation of oxide particles, as seen in the FESEM micrographs (Fig. 3B, sample calcined at 300 °C, Fig. 3C, sample calcined at 400 °C and Fig. 3D, sample calcined at 350 and 450 °C). In order to further analyze these changes, N_2 physisorption at 77 K was employed to study the textural properties of the catalysts, while TEM was used to analyze both the size and morphology of the primary nanoparticles that form the larger octahedra. As observed in Fig. S1,† the size of the primary nanoparticles is also highly affected by the temperature of treatment. The material calcined at 300 °C (Cu_2O/CuO = 0.42) shows the smallest particle size of around 9–15 nm, and the particle size increases with the temperature of calcination and, subsequently, the CuO content. Consequently, the Cu_2O/CuO = 0.15 catalyst presents a particle size between 25 and 50 nm, while the Cu_2O/CuO = 0.01 catalyst has the largest particle size, with a particle size between 45 and 100 nm. Similar to what was also observed in other studies,[25] the particle size follows an opposite trend of the Cu_2O content, the higher the Cu_2O content, the smaller the particle size. However, these differences in particle size are not reflected in the textural properties. As shown in the N_2 physisorption isotherms at 77 K (Fig. S2†), the adsorption of the MOF material drastically drops after its calcination. All the catalysts display very low adsorption profiles, indicating a very low porosity with BET surface areas of around 10 $m^2\ g^{-1}$ in all cases.

The catalytic activity of the materials was assessed for the reduction of 4-nitrophenol to 4-aminophenol using $NaBH_4$ at 25 °C, both with and without irradiation by blue LEDs (see the conversion of the different materials in Fig. S3–S5†). The rate constants were obtained from the slopes of the $\ln(C_0/C)$ *versus* time plot, which corresponds to pseudo-first-order kinetics. Fig. 4A represents the experiments conducted under blue-LED irradiation, while Fig. 4B compares those results with the non-irradiated experiments (see Fig. S3–S5† for all the $\ln(C_0/C)$ *versus* time plots).[26]

The sample obtained by calcination at 400 °C, which has an intermediate Cu_2O/CuO molar ratio of 0.15, exhibits the best performance under both light and dark conditions, suggesting an optimal catalyst composition for this reaction. Interestingly, the use of the sample obtained by calcination at 400 °C exhibits a three-fold increase in the rate constant under dark conditions compared to the sample with either a higher Cu_2O/CuO ratio (calcined at 300 °C, 0.42) or a lower Cu_2O/CuO ratio (calcined at 350/450 °C with a Cu_2O/CuO ratio of only 0.01). To understand the origin of this optimal composition, XPS analyses were performed on the catalysts after one reaction cycle (Fig. S6†). During catalysis, the surface of the materials is modified with a highly reducing agent such as $NaBH_4$, which leads to the formation of Cu_2O and/or Cu. These two oxidation states are difficult to distinguish by the Cu $2p_{3/2}$ XPS spectra. Furthermore, a peak at 933.8 eV, corres-

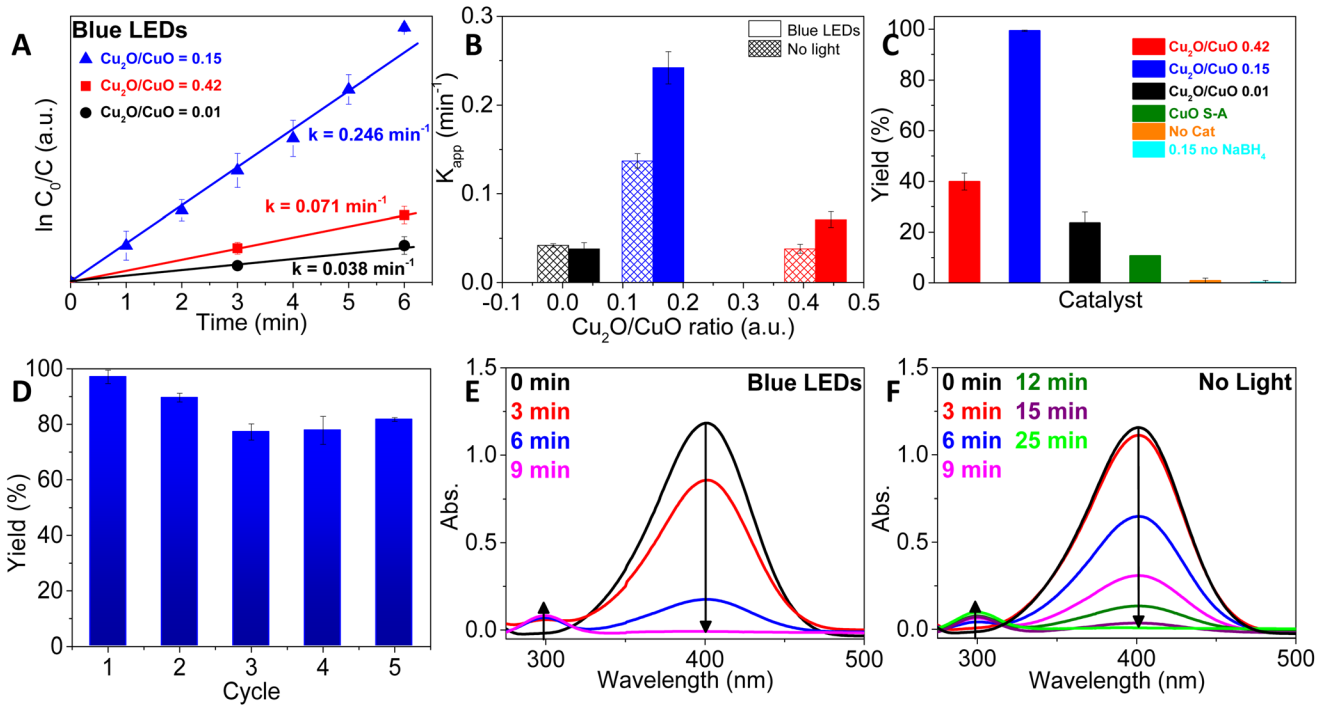

Fig. 4 Catalytic performance of the MOF-derived copper oxides. (A) ln(C_0/C) *versus* time plot, for pseudo-first-order kinetics. (B) Rate constants of the hydrogenation of the three catalysts studied under both dark and blue-LED light conditions. (C) Conversion rates of the three Cu_2O/CuO catalysts studied, a commercial CuO sample, the experiments without a catalyst and without $NaBH_4$, all values taken after 9 min under blue-LED irradiation. (D) Recyclability study using Cu_2O/CuO = 0.15 as the catalyst; the conversion at 25 min of the different photocatalytic cycles is shown in the plot. Evolution of UV-vis absorption in the 250 to 500 nm range of the nitrophenolate ion under (E) blue-LED light irradiation and (F) dark conditions.

ponding to CuO, is also detected in all three samples, albeit in much lower amounts compared to the initial catalysts. As expected, the addition of $NaBH_4$ to the reaction mixtures caused a significant change in the Cu_2O/CuO ratios on the surface of the catalysts. This was due to the reduction of both oxides, which led to the formation of Cu(0) through the reduction of Cu_2O, while at the same time, Cu_2O was regenerated as a result of the reduction of CuO. The presence of Cu(0) and the reduction of oxygen in the lattice were confirmed by XPS (see the Cu LMM spectra in Fig. S7† and the O 1s spectra in Fig. S8† and their descriptions below). These results indicate that a small fraction of Cu(0) is generated *in situ* on the surface during catalysis. The *in situ* formation of these highly active Cu(0) species during the reaction has been reported elsewhere.[27] In those studies, it was concluded that these are the active species for the nitroarene reduction. On the other hand, the presence of CuO after reaction in this reductive medium is unexpected; however, the oxygen dissolved in the aqueous medium and/or the high alkalinity of the solution may contribute to the oxidation of Cu(0) or Cu_2O to CuO, as described elsewhere.[28] Under the reaction conditions, catalysts present a combination of the three states Cu(0), Cu(I) and Cu(II) in different proportions, which are related to their initial composition. The best performing catalyst should have a balanced Cu/Cu_2O/CuO ratio that favors the formation and cyclic regeneration of the active species, which is Cu(0), in order to achieve an optimal rate constant value. Furthermore, the literature extensively describes how the increased number of oxygen vacancies (O_v) in these catalysts can enhance nitroarene adsorption, ultimately improving the catalyst's performance.[10] To quantify the number of oxygen vacancies (O_V) present in our catalysts, we analyzed the O 1s spectra of all materials before and after the reaction. The broad O 1s bands were deconvoluted into three peaks (Fig. S8†). The peak at *ca.* 529.7–530.3 eV can be assigned to the lattice oxygen (O_L) in the Cu_2O/CuO materials. The second peak at 531.2 eV has been described as the result of the ionization of oxygen species due to the compensation of the oxygen deficiencies in the copper oxides, so it can be related to the oxygen vacancies (O_V).[24] The last peak, centred at *ca.* 533.0 eV, is caused by weakly adsorbed oxygen species (O_A), attributed to water adsorbed on the catalyst. The relative concentrations of the various oxygen species on the materials' surface were calculated by determining the area under the corresponding curve (Table S1†). Interestingly, the percentage of O_V in the best performing catalyst is slightly higher than that in the other solids, even after the reconstruction of the catalysts' surface that occurs during the reaction, which may contribute to its superior activity. It is worth noting that even after the reaction, the O_L signal decreases but does not completely disappear. This observation confirms the presence of Cu_2O/CuO in the highly reductive reaction medium.

When comparing rate constants using the same catalysts under light and dark conditions, it is evident that the presence

of Cu_2O plays a critical role in enhancing the catalytic performance (as depicted in Fig. 4B). Interestingly, regardless of the initial Cu_2O/CuO ratio in the catalyst (0.15 or 0.42), the rate constant of reactions carried out under blue-LED light exhibits a two-fold improvement compared to the same experiment performed under dark conditions. The significant variation in activity observed between blue-LED irradiation and dark conditions is apparent from the gradual reduction in the maximum absorption of the nitrophenolate ion (as illustrated in Fig. 4E and F). Using Cu_2O/CuO heterojunctions, the disappearance of the UV-band occurs within 9 minutes in the presence of light, whereas the process slows down considerably to 25 minutes in the dark. In contrast, the sample mainly composed of CuO (Cu_2O/CuO = 0.01) exhibits similar rate constants with and without irradiation, with values significantly lower than those obtained from nitro photoreduction with the other two samples. Here, it is worth highlighting that Cu_2O/CuO materials have previously shown improved catalytic performances compared to those shown for a single phase of CuO or Cu_2O for other reactions, *i.e.* C–N coupling,[29] CO oxidation,[30,31] trichlorosilane synthesis,[32] and NO reduction,[33] among others. Although the use of Cu_2O/CuO heterojunctions has been previously described for the catalytic hydrogenation of nitroarenes,[34–36] to the best of our knowledge, this study is the first example of the use of these Cu_2O/CuO heterojunctions for the photocatalytic reduction of nitroarenes.

Various mechanisms have been proposed for the reduction of nitrophenol to aminophenol using borohydride as a reducing agent.[37] Most of these mechanisms describe the initial adsorption of the reducing agent on the catalyst's surface and the subsequent transfer of hydrogen ions/atoms or electrons from the borohydride to the nitrophenolate ion, induced by the catalyst. This mechanism is similar to what occurs in the hydrolysis of borohydride. So, analyzing the effect of blue-LED light irradiation on the borohydride hydrolysis could provide valuable insights into the influence of this factor on the photocatalyzed reduction of nitroarenes under the studied conditions.[38] Therefore, we evaluated the best performing catalyst, *i.e.*, the Cu_2O/CuO = 0.15 catalyst, in sodium borohydride decomposition, under blue-LED light and dark conditions, by measuring the evolution of hydrogen. Fig. S9† shows that experiments conducted under light decompose sodium borohydride two times faster than experiments conducted in the dark, which can explain the beneficial effect of light in the nitrophenol reduction as well. Similar to the observations made during borohydride hydrolysis, the rate constants for the reduction of 4-nitrophenol are also twice as large in the presence of light as compared to the processes conducted without light. The positive effect of light on the hydrolysis of borohydrides has also been observed for other photocatalysts, leading to similar conclusions.[39–41]

Furthermore, the stability and reusability of the best performing catalyst (Cu_2O/CuO = 0.15) were evaluated under blue-LED light conditions, as shown in Fig. 4D. The material consistently demonstrated excellent performance for five consecutive cycles without a significant loss in activity, maintaining conversion rates of at least 70% throughout. In order to determine the stability of the catalyst over cycles, we have analyzed the catalyst's surface composition after each photocatalytic cycle (Fig. S10†). As shown by the XPS Cu2p3 spectra, the percentages of Cu(I) and Cu(II) do not change drastically so, we can conclude that this catalyst is not only reusable, but also quite stable for at least 5 cycles. However, it is worth noting that the cycles in which the conversion decreases (cycles 2 and 3) are associated with an increase in the Cu(II) content; however, when the Cu(II) content decreases again, the conversion increases. As previously described, under our reaction conditions, the catalysts present a combination of the three states Cu(0), Cu(I) and Cu(II) in different proportions. Thus, the conversion rate depends on the Cu/Cu_2O/CuO ratio, with higher amounts of CuO leading to lower rates. This is the same conclusion that can be drawn from the recycling experiments.

We also performed four control experiments, specifically, (1) a blank experiment, without a catalyst, which did not yield any appreciable amount of 4-aminophenol (Fig. 4C). This observation confirms that $NaBH_4$ alone cannot reduce 4-nitrophenol under the studied conditions, which is likely due to the high kinetic barrier of this reaction.[42] (2) The evaluation of a commercial CuO sample as a benchmark catalyst. This experiment resulted in lower performance compared to our catalysts (Fig. 4C), indicating the high catalytic activity of the MOF-derived solids. (3) An experiment without the use of $NaBH_4$, which showed no conversion of 4-nitrophenol. This experiment shows the need for the presence of an agent capable of contributing hydrogen to the catalytic system in order to achieve the reduction of the nitro group. In our case, this agent is sodium borohydride, but other compounds can be used, such as formic acid, which as can be seen would also be crucial for the reduction to take place.[43,44] (4) With the aim of obtaining a higher proportion of Cu_2O in the Cu_2O/CuO catalyst, we also evaluated the calcination of the MOF at a lower temperature (250 °C), which was insufficient to cause the oxidation of the MOF.

Finally, to assess the selectivity of the best performing catalyst (Cu_2O/CuO = 0.15) towards the reduction of nitro groups in the presence of other functional groups, various substituted nitroarenes were tested. As shown in Table 1, selectivities nearly 100% were obtained in every case at very high conversions (>70%). Entries 1 and 2 demonstrate that the presence of a hydroxy group results in similar conversion values for both isomers, regardless of the relative position of the ring substituents (*ortho* or *para*). The excellent performance of our photocatalyst is evidenced with these examples, where almost quantitative conversions are obtained in a short time (9 min) and under mild conditions, even taking into account that the substitution of an electron donor group (as the –OH) at the *ortho* and *para* positions can increase the electron density at the nitro group by the resonance effect, which should hinder the reduction of the nitro group.[45] In the case of substituents with carbonyl functional groups, the easily reducible functionalities, such as –COOH and –$CONH_2$ (entries 3 and 4), remained

Table 1 Yields and selectivities for the nitro-hydrogenation of nitroarenes under blue LED irradiation with various functionalities and substitution positions in the aromatic ring. Experimental conditions: 10 mg of Cu_2O/CuO = 0.15, 135 mL of a 7.4 × 10^{-2} mM nitroarene solution and 20 mL of a 0.06 M solution of $NaBH_4$ in water. 100 rpm magnetic stirring at 25 °C

Entry	Reagent	Product	Yield (%)	Selectivity (%)
1	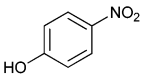	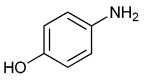	99	100
2	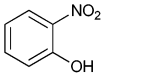	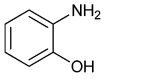	97	100
3	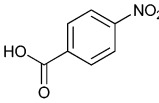	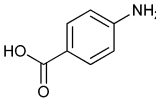	70	100
4	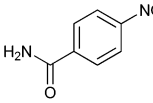	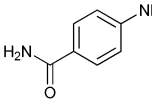	90	100

unaffected.[46] However, as shown in Table 1, the conversion falls moderately with respect to that of nitrophenols.

Conclusions

Tunable heterojunctions of copper oxides (Cu_2O/CuO) were prepared by the controlled thermal oxidation of the Cu(BTC) MOF. Through this simple approach, we were able to assess the presence of an optimum Cu_2O/CuO ratio for the hydrogenation of 4-nitrophenol with $NaBH_4$ under light or dark conditions. Irradiation with blue-LED light causes a two-fold increase in the performance of the heterojunctions, which can be, partially, ascribed to faster sodium borohydride decomposition in the presence of light. The best performing catalyst retained its activity during 5 catalytic cycles and displayed excellent selectivity towards the amine in systems containing both nitro groups and other functionalities such as –COOH or –OH. These results show how Cu_2O/CuO heterojunctions can be used as effective, inexpensive, and non-toxic alternatives to noble metals for the selective and stable reduction of nitroarenes.

Author contributions

This manuscript was written through contributions from all authors. All authors have given approval to the final version of the manuscript.

Conflicts of interest

There are no conflicts to declare.

Acknowledgements

The authors thank the Spanish Ministry of Science and Innovation and AEI/FEDER, UE for funding through the projects refs. RTI2018-099504-B-C21 and PID2021-128761OB-C21. This project has received funding from the Generalitat Valenciana under project ref. AICO/2021/132.

References

1 A. Corma and P. Serna, Chemoselective hydrogenation of nitro compounds with supported gold catalysts, *Science*, 2006, **313**, 332–334.
2 J. Feng, L. Su, Y. Ma, C. Ren, Q. Guo and X. Chen, $CuFe_2O_4$ magnetic nanoparticles: A simple and efficient catalyst for the reduction of nitrophenol, *Chem. Eng. J.*, 2013, **221**, 16–24.
3 V. R. Choudhary, M. G. Sane and S. S. Tambe, Kinetics of hydrogenation of o-nitrophenol to o-aminophenol on Pd/carbon catalysts in a stirred three-phase slurry reactor, *Ind. Eng. Chem. Res.*, 1998, **37**, 3879–3887.
4 H. J. Yang, M. Redington, D. P. Miller, E. Zurek, M. Kim, C. S. Yoo, S. Y. Lim, H. Cheong, S. A. Chae, D. Ahn and N. H. Hur, New monoclinic ruthenium dioxide with highly selective hydrogenation activity, *Catal. Sci. Technol.*, 2022, 6556–6565.
5 H. U. Blaser, H. Steiner and M. Studer, Selective catalytic hydrogenation of functionalized nitroarenes: An update, *ChemCatChem*, 2009, **1**, 210–221.
6 J. J. Corma, S. Avelino, C. Pedro and C. Patricia, Transforming Nonselective into Chemoselective Metal Catalysts for the Hydrogenation of Substituted Nitroaromatics, *J. Am. Chem. Soc.*, 2008, **130**, 8748–8753.
7 J. Zhou, W. Hou, X. Liu and D. Astruc, Pd, Rh and Ru nanohybrid-catalyzed tetramethyldisiloxane hydrolysis for H2 generation, nitrophenol reduction and Suzuki-Miyaura cross-coupling, *Inorg. Chem. Front.*, 2022, **9**, 1416–1422.
8 J. Song, Z. F. Huang, L. Pan, K. Li, X. Zhang, L. Wang and J. J. Zou, Review on selective hydrogenation of nitroarene by catalytic, photocatalytic and electrocatalytic reactions, *Appl. Catal., B*, 2018, **227**, 386–408.
9 M. C. Bryan, P. J. Dunn, D. Entwistle, F. Gallou, S. G. Koenig, J. D. Hayler, M. R. Hickey, S. Hughes, M. E. Kopach, G. Moine, P. Richardson, F. Roschangar, A. Steven and F. J. Weiberth, Key Green Chemistry research areas from a pharmaceutical manufacturers' perspective revisited, *Green Chem.*, 2018, **20**, 5082–5103.
10 K. Rajendran, N. Pandurangan, C. P. Vinod, T. S. Khan, S. Gupta, M. A. Haider and D. Jagadeesan, CuO as a reactive and reusable reagent for the hydrogenation of nitroarenes, *Appl. Catal., B*, 2021, **297**, 120417.
11 Y. Huang, K. Zheng, X. Liu, X. Meng and D. Astruc, Optimization of Cu catalysts for nitrophenol reduction, click reaction and alkyne coupling, *Inorg. Chem. Front.*, 2020, **7**, 939–945.

12 G. Ren, H. Han, Y. Wang, S. Liu, J. Zhao, X. Meng and Z. Li, Recent advances of photocatalytic application in water treatment: A review, *Nanomaterials*, 2021, **11**, 1804.
13 Y. Shiraishi, Y. Togawa, D. Tsukamoto, S. Tanaka and T. Hirai, Highly efficient and selective hydrogenation of nitroaromatics on photoactivated rutile titanium dioxide, *ACS Catal.*, 2012, **2**, 2475–2481.
14 Y. Shiraishi, H. Hirakawa, Y. Togawa, Y. Sugano, S. Ichikawa and T. Hirai, Rutile crystallites isolated from degussa (Evonik) P25 TiO_2: Highly efficient photocatalyst for chemoselective hydrogenation of nitroaromatics, *ACS Catal.*, 2013, **3**, 2318–2326.
15 H.-q. Jiang, H. Endo, H. Natori, M. Nagai and K. Kobayashi, Fabrication and efficient photocatalytic degradation of methylene blue over CuO/$BiVO_4$ composite under visible-light irradiation, *Mater. Res. Bull.*, 2009, **44**, 700–706.
16 Y. Wang, D. Huang, X. Zhu, Y. Ma, H. Geng, Y. Wang, G. Yin, D. He, Z. Yang and N. Hu, Surfactant-free synthesis of Cu2O hollow spheres and their wavelength-dependent visible photocatalytic activities using LED lamps as cold light sources, *Nanoscale Res. Lett.*, 2014, **9**, 36–38.
17 H. G. Kim, P. H. Borse, W. Choi and J. S. Lee, Photocatalytic nanodiodes for visible-light photocatalysis, *Angew. Chem., Int. Ed.*, 2005, **44**, 4585–4589.
18 S. Sun, X. Zhang, J. Zhang, L. Wang, X. Song and Z. Yang, Surfactant-free CuO mesocrystals with controllable dimensions: Green ordered-aggregation-driven synthesis, formation mechanism and their photochemical performances, *CrystEngComm*, 2013, **15**, 867–877.
19 K. S. Lin, A. K. Adhikari, C. N. Ku, C. L. Chiang and H. Kuo, Synthesis and characterization of porous HKUST-1 metal organic frameworks for hydrogen storage, *Int. J. Hydrogen Energy*, 2012, **37**, 13865–13871.
20 C. C. Chusuei, M. A. Brookshier and D. W. Goodman, Correlation of relative X-ray photoelectron spectroscopy shake-up intensity with CuO particle size, *Langmuir*, 1999, **15**, 2806–2808.
21 R. Gil-San-Millan, A. Grau-Atienza, D. T. Johnson, S. Rico-Francés, E. Serrano, N. Linares and J. García-Martínez, Improving hydrogen production from the hydrolysis of ammonia borane by using multifunctional catalysts, *Int. J. Hydrogen Energy*, 2018, **43**, 17100–17111.
22 T. Degen, M. Sadki, E. Bron, U. König and G. Nénert, The high score suite, *Powder Diffr.*, 2014, **29**, S13–S18.
23 L. Debbichi, M. C. Marco De Lucas, J. F. Pierson and P. Krüger, Vibrational properties of CuO and Cu 4O 3 from first-principles calculations, and Raman and infrared spectroscopy, *J. Phys. Chem. C*, 2012, **116**, 10232–10237.
24 S. Poulston, P. M. Parlett, P. Stone and M. Bowker, Surface Oxidation and Reduction of CuO and Cu_zO Studied Using XPS and XAES, *Surf. Interface Anal.*, 1996, **24**, 811–820.
25 F. Bayat and S. Sheibani, Enhancement of photocatalytic activity of CuO-Cu_2O heterostructures through the controlled content of Cu2O, *Mater. Res. Bull.*, 2022, **145**, 111561.
26 X. Zhang, X. He, Z. Kang, M. Cui, D. P. Yang and R. Luque, Waste Eggshell-Derived Dual-Functional CuO/ZnO/Eggshell Nanocomposites: (Photo)catalytic Reduction and Bacterial Inactivation, *ACS Sustainable Chem. Eng.*, 2019, **7**, 15762–15771.
27 A. Saha and B. Ranu, Highly chemoselective reduction of aromatic nitro compounds by copper nanoparticles/ammonium formate, *J. Org. Chem.*, 2008, **73**, 6867–6870.
28 A. K. Sasmal, S. Dutta and T. Pal, A ternary Cu_2O-Cu-CuO nanocomposite: A catalyst with intriguing activity, *Dalton Trans.*, 2016, **45**, 3139–3150.
29 A. K. Kar and R. Srivastava, Selective synthesis of Cu–Cu2O/C and CuO–Cu2O/C catalysts for Pd-free C–C, C–N coupling and oxidation reactions, *Inorg. Chem. Front.*, 2019, **6**, 576–589.
30 B. Wei, N. Yang, F. Pang and J. Ge, Cu_2O-CuO hollow nanospheres as a heterogeneous catalyst for synergetic oxidation of CO, *J. Phys. Chem. C*, 2018, **122**, 19524–19531.
31 Y. Yang, H. Dong, Y. Wang, Y. Wang, N. Liu, D. Wang and X. Zhang, A facile synthesis for porous CuO/Cu_2O composites derived from MOFs and their superior catalytic performance for CO oxidation, *Inorg. Chem. Commun.*, 2017, **86**, 74–77.
32 Z. Yang, T. Kang, Y. Ji, J. Li, Y. Zhu, H. Liu, X. Jiang, Z. Zhong and F. Su, Architectural Cu2O@CuO mesocrystals as superior catalyst for trichlorosilane synthesis, *J. Colloid Interface Sci.*, 2021, **589**, 198–207.
33 X. Wu, H. Meng, Y. Du, J. Liu, B. Hou and X. Xie, Insight into Cu_2O/CuO collaboration in the selective catalytic reduction of NO with NH3: Enhanced activity and synergistic mechanism, *J. Catal.*, 2020, **384**, 72–87.
34 K. Sahu, B. Satpati, R. Singhal and S. Mohapatra, Enhanced catalytic activity of CuO/Cu_2O hybrid nanowires for reduction of 4-nitrophenol in water, *J. Phys. Chem. Solids*, 2020, **136**, 109143.
35 J. Li, W. Liu, Y. Ding, L. Liu, F. Li and Q. Li, Composition modulation of Cu/Cu_2O/CuO nanoparticles supported on carbon for p-nitrophenol reduction, *Korean J. Chem. Eng.*, 2019, **36**, 851–859.
36 T. Zhu, Q. He, Z. Wang, J. Zhang, H. Li, H. Fu and F. Liao, Self-driven in situ facile synthesis of CuO/Cu2O for enhanced catalytic reduction of 4-nitrophenol by acetic acid, *New J. Chem.*, 2022, **46**, 15911–15918.
37 T. Aditya, A. Pal and T. Pal, Nitroarene reduction: a trusted model reaction to test nanoparticle catalysts, *Chem. Commun.*, 2015, **51**, 9410–9431.
38 M. M. Mohamed and H. El-Farsy, Rapid reduction of nitroarenes photocatalyzed by an innovative Mn3O4/α-Ag2WO4 nanoparticles, *Sci. Rep.*, 2020, **10**, 1–18.
39 N. A. M. Barakat, Catalytic and photo hydrolysis of ammonia borane complex using Pd-doped Co nanofibers, *Appl. Catal., A*, 2013, **451**, 21–27.
40 R. Helmy, G. A. El-Inany, H. S. Seleem, M. O. Abdel-Salam, T. Yoon and M. Saif, A novel Dy3+ modified Zn2Ti3O8 nanoparticles for efficient hydrogen production photocatalysis, *J. Alloys Compd.*, 2022, **907**, 164487.

41 X. Lin, Q. Li and Y. Pang, Hydrogen generation from photocatalytic hydrolysis of alkali-metal borohydrides, *Int. J. Energy Res.*, 2017, **41**, 1342–1350.
42 J. Rong, F. Qiu, T. Zhang, Y. Zhu, J. Xu, Q. Guo and X. Peng, Non-noble metal@carbon nanosheet derived from exfoliated MOF crystal as highly reactive and stable heterogeneous catalyst, *Appl. Surf. Sci.*, 2018, **447**, 222–234.
43 Z. Yin, L. Xie, S. Cao, Y. Xiao, G. Chen, Y. Jiang, W. Wei and L. Wu, Ag/Ag2O confined visible-light driven catalyst for highly efficient selective hydrogenation of nitroarenes in pure water medium at room temperature, *Chem. Eng. J.*, 2020, **394**, 125036.
44 Z. Yin, Y. Xiao, X. Wan, Y. Jiang, G. Chen, Q. Shi and S. Cao, High photocatalytic activity of Cu2O embedded in hierarchically hollow SiO_2 for efficient chemoselective hydrogenation of nitroarenes, *J. Mater. Sci.*, 2021, **56**, 3874–3886.
45 V. Vinod Kumar, A. Dharani, M. Mariappan and S. P. Anthony, Synthesis of CuO and Cu 2 O nano/microparticles from a single precursor: effect of temperature on CuO/Cu_2O formation and morphology dependent nitroarene reduction, *RSC Adv.*, 2016, **6**, 85083–85090.
46 R. Dey, N. Mukherjee, S. Ahammed and B. C. Ranu, Highly selective reduction of nitroarenes by iron(0) nanoparticles in water, *Chem. Commun.*, 2012, **48**, 7982–7984.